COMMUNICATIONS IN SCIENCE AND TECHNOLOGY
Homepage: cst.kipmi.or.id

Green synthesis of mixed-phase copper nanostructures using *Annona muricata* extract: role of oxidation on selective antifungal activity

Nurjanah[a], Irfan Mustafa[b], Tasya Ulfika[a,b], Binawati Ginting[a,b], Ilham Maulana[a,b,*]

[a] *Department of Chemistry, Universitas Syiah Kuala, Banda Aceh 23111, Indonesia*
[b] *Master Program of Chemistry, Universitas Syiah Kuala, Banda Aceh 23111, Indonesia*

Article history:
Received: 23 April 2026 / Received in revised form: 10 June 2026 / Accepted: 19 June 2026

Abstract

The green synthesis of copper-based nanomaterials utilizing plant extracts has attracted significant attention; however, controlling oxidation state and understanding its impact on biological performance remain challenging. In this present study, mixed-phase copper nanostructures were synthesized using aqueous stem bark extract of *Annona muricata* as a dual reducing and stabilizing agent under mild conditions. Phytochemical analysis revealed a high total phenolic content (310 mg GAE/g), thus confirming the strong redox capability for Cu^{2+} reduction. UV–Vis spectroscopy indicated the formation of nanoparticle with a characteristic absorption band at approximately 360 nm. XRD and EDS analyses were conducted to confirm the coexistence of Cu (0), Cu_2O, and CuO phases. The crystallite sizes of these phases ranged from 22 to 28 nm, thereby suggesting partial oxidation during synthesis. The utilization of Fourier-transform infrared spectroscopy (FTIR) analysis has been demonstrated to be a valuable tool in the identification of the involvement of polyphenolic functional groups in reduction and surface stabilization processes. SEM and TEM observations revealed the presence of quasi-spherical nanoparticles with a mean diameter of 4 -16 nm, exhibiting signs of partial aggregation. The antimicrobial performance of the synthesized nanostructures exhibited a concentration-dependent response. While limited antibacterial activity was observed against *Staphylococcus aureus* and *Escherichia coli*, a pronounced antifungal effect was obtained against *Candida albicans* with an inhibition zone of 27.81 mm at 20% concentration. The pronounced antifungal activity exhibited a strong correlation with the presence of mixed copper phases, suggesting that the oxidation-induced surface chemistry and controlled Cu^{2+} ion availability may contribute significantly to the observed efficacy. These findings highlight the functional role of oxidation in plant-mediated copper nanostructures and demonstrate their potential as selective antifungal agents. This work provides insight into the relationship between phase composition and biological activity in green-synthesized copper nanomaterials. The remarkable selectivity exhibited by these mixed-phase nanostructures against fungal pathogens positions them as a viable, eco-friendly alternative for targeted antifungal applications, thus overcoming the limitations of conventional non-specific antimicrobial agents.

Keywords: Green synthesis; copper nanoparticles; *annona muricata*; phytochemical reduction; antimicrobial activity

1. Introduction

Copper-based nanoparticles have been the focus of increasing interest due to the wide range of applications of these particles including catalytic, optical, antimicrobial, and environmental uses. A comparison of copper with noble metals such as silver and gold, reveals significant economic advantages and comparable redox activity, thus making it an attractive candidate for the large-scale production of nanomaterial [1,2]. However, a major limitation of copper nanoparticles lies is their inherent instability and high susceptibility to oxidation, which frequently results in the formation of mixed-phase materials (Cu, Cu_2O, CuO) with altered physicochemical and biological properties [3,4]. The issue of controlling oxidation during synthesis remains a critical challenge, particularly under ambient conditions [5]. Conventional chemical and physical synthesis routes frequently rely on hazardous reducing agents, elevated temperatures, and complex stabilization systems, raising concerns regarding environmental impact, cost, and sustainability [6–8]. In response, plant-mediated green synthesis has emerged as an eco-friendly alternative, utilizing phytochemicals such as phenolics, flavonoids, terpenoids, and alkaloids as natural reducing and capping agents [9,10]. These bioactive molecules donate electrons to metal ions, hence facilitating nucleation and nanoparticle formation while simultaneously stabilizing the formed particles through mechanisms such as chelation and surface adsorption [11]. Amongst the medicinal plants studied, *A. muricata* (soursop) is found to be rich in polyphenolic compounds and secondary metabolites with strong antioxidant properties [12,13]. It has been demonstrated in previous studies that the green synthesis of copper nanoparticles has been successful when various plant

* Corresponding author.
Email: ilham.maulana@usk.ac.id
https://doi.org/10.21924/cst.11.1.2026.1967

extracts have been utilized; however, is a paucity of reports focusing on stem bark extract of *A. muricata* [14–16]. Furthermore, there are only small number of studies systematically correlating phytochemical content, oxidation behavior, crystalline phase formation, and antimicrobial performance in copper-based nanomaterials synthesized under aqueous conditions [17,18]. Antimicrobial resistance represents a growing global health concern, prompting the exploration of alternative antimicrobial agents. In this context, various nanomaterials, including multi-phase composites and functionalized coatings, have been extensively engineered to suppress bacterial growth and optimize biocompatibility [19,20]. It has been established that copper nanoparticles exhibit antimicrobial activity through multiple mechanisms, including the generation of reactive oxygen species (ROS), the disruption of cell membranes, the denaturation of proteins, and the controlled release of Cu^{2+} ions [21]. Nevertheless, antimicrobial efficacy is highly reliant upon the phase composition of the nanoparticle, particle size, surface chemistry, and stability against oxidation [21,22]. While previous studies on *A. muricata*-mediated copper nanoparticles primarily report single-phase CuO systems for anticancer or antibacterial applications [23,24], the deliberate preparation of mixed-phase copper nanostructures under ambient conditions remains less explored. In this work, instead of completely suppressing the oxidation, we utilized the natural ambient oxidation technique to intentionally synthesize a mixed-phase $Cu/Cu_2O/CuO$ system. This approach facilitates the investigation of how the coexistence of these distinct oxidation states drives a highly selective antifungal performance against *Candida albicans*, thereby clarifying the specific functional role of partial oxidation in tuning biological activity.

The objectives of this study include firstly the investigation of the formation of mixed-phase copper nanostructures mediated by the aqueous stem bark extract of *A. muricata* under ambient oxidation; secondly, the characterization of the structural and physicochemical properties of the synthesized nanoparticles, thirdly, evaluation of the relationship between phytochemical content and nanoparticle formation, and fourthly the assessment of their antimicrobial activity against representative Gram-positive, Gram-negative, and fungal strains. By examining phase composition and oxidation behavior, this work provides insight into the performance limitations of plant-mediated copper nanoparticles and suggests strategies for improving their functional stability.

2. Materials and Methods

2.1. Materials

Fresh stem bark of *Annona muricata* was collected from Darussalam District, Aceh Besar Regency. The Copper (II) sulfate pentahydrate ($CuSO_4.5H_2O$, ≥99.5%) was employed as the copper precursor for the synthesis of nanoparticle. Folin–Ciocalteu reagent, gallic acid ($C_7H_6O_5$, 98% purity), sodium carbonate (Na_2CO_3, ≥99.5% purity), aluminum chloride ($AlCl_3$, 98% purity), quercetin (≥95% purity), potassium acetate (CH_3COOK, ≥99.0% purity), and methanol (CH_3OH, analytical grade, 99.8% purity) were utilized for phytochemical quantification assays. Throughout the course of experiments, distilled water (aquadest) was utilized. The antimicrobial evaluation was conducted using Mueller–Hinton Agar (MHA) and Nutrient Agar (NA) for bacterial cultures, and Potato Dextrose Agar (PDA) for fungal growth. The microbial strains utilized in this study, including *Staphylococcus aureus*, *Escherichia coli*, and *Candida albicans,* were obtained from the laboratory collection of the Faculty of Medicine, Syiah Kuala University. Chloramphenicol (30 µg), and nystatin (100 µg) from HiMedia served as positive controls for the antibacterial and antifungal assays, respectively.

2.2. Preparation of A. muricata stem bark extract

The dried stem bark of *A. muricata* was ground into a coarse powder prior to extraction. Approximately 150 g of the powdered material was extracted with 900 mL of distilled water at 70 °C for 30 minutes under continuous magnetic stirring. The extraction process was conducted with the objective of facilitating the release of water-soluble phytochemicals, including phenolic and flavonoid compounds. Subsequent to extraction, the mixture was filtered using Whatman No. 1 filter paper to separate the solid residue from the aqueous filtrate. The collected filtrate was subsequently concentrated under reduced pressure using a rotary vacuum evaporator at controlled temperature to obtain the crude aqueous stem bark extract. The extraction yield (%) was calculated based on the dry weight of the extract relative to the initial dry plant material (see Fig. 1). The obtained extract was stored at 4 °C until further use for nanoparticle synthesis and phytochemical analysis. The Total Phenolic Content (TPC) was subsequently determined using the Folin–Ciocalteu method.

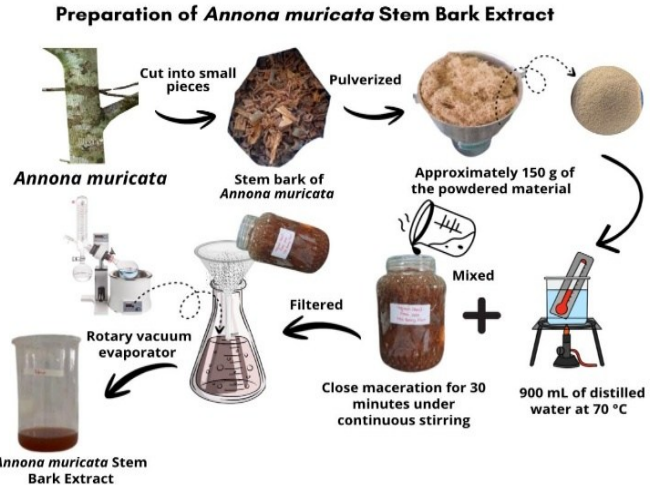

Fig. 1. Mechanism preparation of *A. muricata* stem bark extract

2.3. Biosynthesis of copper-based nanoparticles

The synthesis of copper-based nanoparticles was accomplished via a plant-mediated reduction method utilizing the aqueous stem bark extract of *A. muricata* (AM extract). In summary, 100 mL of the prepared extract was added dropwise to 400 mL of 0.1 M copper (II) sulfate ($CuSO_4$) solution under continuous magnetic stirring at ambient temperature (25 ± 2 °C), maintaining an extract-to-precursor volume ratio of 1:4. The reaction mixture was left to proceed for 24 hours at room

temperature. The formation of nanoparticles was preliminarily indicated by a visible color change in the solution, which was recorded at specific time intervals (30 minutes, 60 minutes, and 24 hours). The reduction process and nanoparticle formation were further monitored using UV–Visible spectroscopy over an appropriate wavelength range. Subsequent to the completion of the reaction, the mixture was subjected to a centrifugal process at a speed of 4,000 rpm for a duration of 15 minutes with the objective of separating the formed nanoparticles. The collected precipitate was washed repeatedly with distilled water to remove unreacted constituents and residual phytochemicals. The precipitate was then dried at controlled temperature to obtain powdered copper-based nanoparticles (AMCuNPs) for subsequent characterization.

2.4. Characterizations

The synthesis of *Annona muricata*-mediated copper-based nanoparticles (AMCuNPs) was characterized by means of complementary spectroscopic and microscopic techniques to evaluate their optical, structural, morphological, and compositional properties. UV–Vis spectra were obtained using a Shimadzu UV–Vis spectrophotometer in the range of 800–200 nm to monitor the reduction of Cu^{2+} ions and nanoparticle formation at different reaction times, where the emergence of characteristic absorption bands indicated surface plasmon resonance behavior. The identification of functional groups with phytochemicals involved in nanoparticle reduction and stabilization was achieved by utilization of the KBr pellet method and Shimadzu FTIR spectrometer in the range of 4000–400 cm^{-1}. A comparative analysis was conducted between the crude extract and synthesized nanoparticles, with a view to elucidate biomolecule–metal interactions. The crystalline structure and phase composition were determined by X-ray diffraction (XRD). For this purpose, a Rigaku Miniflex 600 diffractometer operated at 40 kV was used and the average crystallite size was estimated using the Debye–Scherrer equation, which is based on peak broadening analysis. The surface morphology and aggregation characteristics were examined using Scanning Electron Microscopy (SEM), while the elemental composition and confirmation of copper species were obtained through Energy Dispersive Spectroscopy (EDS) (JEOL JSM-6510LA) operated at 15.00 kV with a magnification of ×3000. The employment of transmission electron microscopy (TEM) was further instrumental in the assessment of the distribution of particle size and the morphology at the nanoscale.

2.5. Thin layer chromatography (TLC) analysis

Thin Layer Chromatography (TLC) was performed to qualitatively assess the phytochemical constituents present in the AM extract. The crude extract was dissolved in distilled water and applied onto silica gel 60 F_{254} TLC plates (6 × 3 cm) using a glass capillary tube. The plates were developed in a solvent system consisting of a 9:1 (v/v) methanol: water mixture within a saturated developing chamber. Following elution, the plates were air-dried and initially visualized under ultraviolet light at 254 nm. Subsequently, the developed plates were sprayed with vanillin reagent as a derivatizing agent and re-examined under UV illumination at 254 nm to enhance spot visualization. The retention factor values (Rf) were calculated for the detected spots using standard methodology.

2.6. Antimicrobial activity

The antimicrobial activity of the synthesized AMCuNPs was evaluated against Gram-positive *Staphylococcus aureus* (ATCC 29213), Gram-negative *Escherichia coli* (ATCC 25922), and the fungal strain *Candida albicans* (ATCC 10231) using the agar disc diffusion method.

2.6.1.Preparation of culture media

Mueller–Hinton Agar (MHA) and Nutrient Agar (NA) were utilized for bacterial assays, while Potato Dextrose Agar (PDA) was employed for fungal evaluation. All culture media were subjected to autoclaving at 121 °C for 20 minutes prior to use to ensure their sterility.

2.6.2.Preparation of microbial inoculum

Bacterial suspensions were prepared from freshly grown cultures and adjusted to match the 0.5 McFarland turbidity standard (approximately 1×10^8 CFU/mL). The optical density was measured at 625 nm using a UV–Vis spectrophotometer, with acceptable absorbance values ranging from 0.08 to 0.10. For *C. albicans*, the inoculum density was standardized spectrophotometrically at 530 nm, with the absorbance values being between 0.50 and 0.60.

2.6.3. Disc diffusion assay

Sterile Petri dishes containing solidified MHA (for bacteria) or PDA (for fungi) were uniformly inoculated with the standardized microbial suspensions using sterile cotton swabs. Sterile paper discs were impregnated with AMCuNPs suspensions at concentrations of 5%, 10%, and 20% (w/v). A 20% $CuSO_4$ solution served as a precursor control. Chloramphenicol discs (for bacteria) and nystatin (for fungi) were utilized as positive controls, while the extraction solvent served as a negative control. The treated plates were then incubated at 37 °C for 24 hours for bacterial strains and 48 h for fungal strains. Subsequent to the process of incubation, the diameter of the inhibition zones was measured in millimeters using a digital caliper. The antibacterial assay was conducted as a single determination because it was intended as a preliminary screening evaluation of the antibacterial potential of the synthesized CuNPs.

3. Results and Discussion`

3.1. Extraction of A. muricata bark

The aqueous extraction of *A. muricata* stem bark yielded 2.87% (w/w) crude extract relative to the initial dry biomass. Despite the moderate extraction yield, the phytochemical analysis revealed a high total phenolic content (TPC) of 310

mg GAE/g extract and a comparatively lower total flavonoid content (TFC) of 2.56 mg QE/g extract. The significantly higher TPC in comparison to the TFC indicates that phenolic compounds represent the dominant class of antioxidant metabolites in the aqueous bark extract (AM extract). This finding aligns with earlier reports on related Annona species and other *Annonaceae* plants, where phenolic compounds were found to be more abundant than flavonoids in aqueous extracts. For instance, the water extract of *Annona squamosa* bark demonstrated TPC and TFC values of 78.28 mg GAE/g and 1.24 mg QE/g, respectively [25]. Similarly, methanolic extracts of *Polyalthia longifolia* roots exhibited a TPC of 35.30 mg GAE/g and TFC of 16.90 mg QE/g [26]. The comparatively higher phenolic content observed in the present study suggests a strong reducing potential of the *A. muricata* bark extract, which may play a critical role in the bioreduction of Cu^{2+} ions during nanoparticle synthesis.

Phenolic compounds are well known for their electron-donating capacity through hydroxyl (–OH) functional groups, facilitating redox reactions and metal ion reduction. Consequently, the elevated TPC value supports the suitability of *A. muricata* stem bark extract as an effective bioreducing and stabilizing agent in the green synthesis of copper-based nanoparticles [10,27].

3.2. Biosynthesis of copper nanoparticles

The initial evidence for the formation of copper nanoparticle formation was observed as a distinct color change in the reaction mixture [28]. The aqueous *A. muricata* extract, which exhibited an orange coloration, gradually transformed to a light green solution upon the addition of $CuSO_4$ under ambient conditions. The transition was monitored at varying reaction intervals (0 minutes, 30 minutes, 1 hour, and 24 hours), as illustrated in Fig. 2. The observed color change suggests the reduction of Cu^{2+} ions and the formation of copper-based nanostructures (AMCuNPs) [29]. Such chromatic variation is commonly attributed to alterations in the electronic structure of copper species and the emergence of nanoscale copper or copper oxide particles [30]. In the context of plant-mediated synthesis systems, this phenomenon is typically associated with surface plasmon resonance (SPR) effects and/or the formation of Cu_2O and CuO phases, which exhibit characteristic optical absorption in the visible region. The gradual stabilization of the green coloration over a-24-hour period indicates the completion of the redox process and nanoparticle growth. These observations confirm that phytochemical constituents present in the AM extract actively participate in the reduction of Cu^{2+} ions and the nucleation of copper-based nanoparticles under mild aqueous conditions.

The UV-Vis absorption spectrum of the AM extract solution demonstrated pronounced absorption in the UV region (<350 nm), indicative of the presence of the phenolic and flavonoid compounds characteristic of plant extract [31]. Following the addition of $CuSO_4$, the reaction mixtures at early intervals (0 minutes, 30 minutes, and 1 hour) exhibited a closely shifting spectral pattern. However, following a 24-hour reaction period, a significant change was observed; the overall change in light absorption increased dramatically across the entire spectrum, accompanied by a board, rising absorption band extending into the visible region (600-800 nm). The presence of a board peak in the spectrum, in addition to the absence of a sharp, well-defined metallic copper Surface Plasmon Resonance (SPR) peak (typically around 570 nm) suggests that the system predominantly consists of copper oxide phases (Cu_2O and CuO) rather than purely metallic copper. The validity of this assertion is further supported by the findings of [32] and Maulana et al. (2022) [26] who reported that the formation of mixed copper oxide phases frequently results in substantial baseline shifts and broad absorption features in the lower wavelength region (300-400 nm) in addition to broad transition at higher wavelengths. It is important to note that, in the lower wavelength region (300–400 nm), this absorption feature significantly overlaps with both the internal electronic transitions of oxidized copper species and the active phytochemical constituents of the extract. This indicates that it represents a combined optical response rather than purely metallic core formation. This mechanism of plant-mediated reduction is consistent with previous findings reported in this journal, which demonstrated the successful fabrication of copper nanoparticles using *Anredera cordifolia* extract [33]. Consequently, these spectrophotometric observations suggest that metallic copper Cu (0) nanoparticles are either present in a very low concentration or have undergone partial oxidation into copper oxide species under ambient aqueous conditions, as further elucidated by XRD and EDS analyses [34].

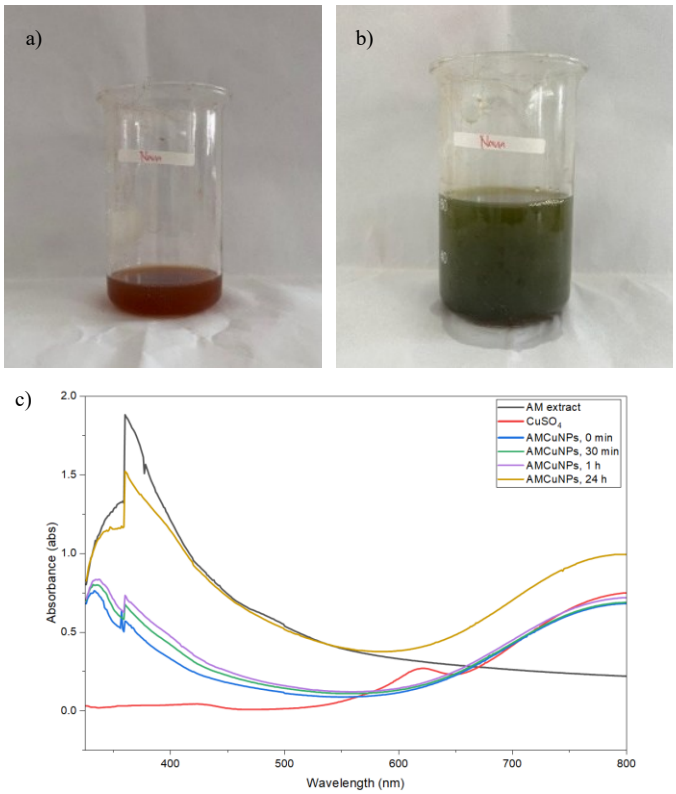

Fig. 2. (a) Orange-colored AM extract solution, (b) Reaction mixture of $CuSO_4$ and AM extract, (c) Analysis results of AM extract and AMCuNPs solution with time variation using UV-Vis spectrophotometer

3.3. Thin layer chromatography (TLC) analysis

Thin Layer Chromatography (TLC) was employed to

qualitatively evaluate the phytochemical changes occurring during the biosynthesis of copper-based nanoparticles. The chromatogram of the crude AM extract exhibited yellow-colored spots under UV illumination after derivatization, thereby confirming the presence of active phenolic and flavonoid compounds. As demonstrated in Fig. 3, the chromatograms obtained from both the $CuSO_4$ precursor track and the synthesized AMCuNPs track exhibited significantly sharper and more intense fluorescent spots in comparison to the crude extract. This phenomenon can be attributed to the strong chelating property of *A. muricata* phytochemicals toward copper ions Cu^{2+}. It has observed that when free flavonoids and phenolics coordinate with copper to form metal-ligand complexes, either as unreacted ions in the $CuSO_4$ mixture or as capping agents bound to the surface of AMCuNPs, their electronic transition states are altered. This metal-coordination effect systematically enhances the fluorescence emission and color intensity under UV light, a well-recognized hyperchromic shift in coordination chemistry.

The distinct enhancement and stabilization of these phytochemical bands in the nanoparticle sample reflect the successful coordination of the bioactive constituents of the extract with the copper core during the redox reaction with $CuSO_4$. This observation supports the proposed mechanism in which phenolic compound donates electrons to Cu^{2+} ions, thereby reducing them into copper-based nanoparticles. Concurrently, the phytochemicals themselves undergo oxidation, resulting in the formation of a protective capping layer. Additionally, the strong adsorption of these oxidized biomolecules onto the nanoparticle surface contributes to the prominent appearance of the chromatographic spots in the AMCuNPs track. The findings provide qualitative evidence that phytochemicals from *A. muricata* actively participate in both the reduction and stabilization processes during green synthesis.

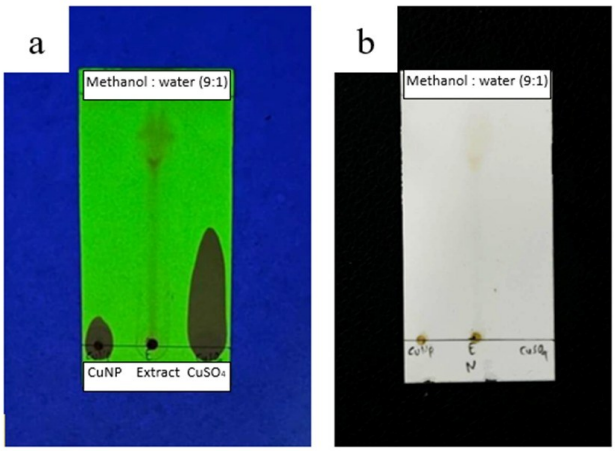

Fig. 3. (a) TLC chromatogram of AM extract, AMCuNPs and $CuSO_4$ solution under UV light at 254 nm, (b) TLC chromatogram after spraying vanillin sulfate

3.4. Fourier transform infrared spectroscopy (FTIR)

The results of FTIR analysis of AMCuNPs demonstrated significant spectral peaks at wavenumbers 3388 cm^{-1} and 2352 cm^{-1}. The prominent and broad absorption band observed at 3388 cm^{-1} is attributed to the O-H stretching vibrations of polyphenolic and flavonoid compounds present in the plant extract [35]. Subsequent to the formation of nanoparticle, a broad O–H band maintains its high intensity in the AMCuNPs spectrum. The persistence of this strong absorption is primarily due to residual moisture or bound water molecules within the biogenic sample, as well as the abundant presence of phytochemical capping agents successfully adsorbed onto the large surface area of the nanoparticles. However, a noticeable shifting and broadening of this peak indicates that the hydroxyl groups are actively involved in hydrogen bonding and coordination during the redox and stabilization processes with the copper species. As evident in the existing literature, there are similarities in the behaviors of hydroxyl group interactions, peak shifting, and structural stabilization within engineered nanomaterials [19,20].

Furthermore, the absorption in peak that was observed at 1620 cm^{-1} is attributed to the C=O stretching of ketones involved in polyphenol bonding with the copper metal. This interaction results in a lower electron density due to electron delocalization towards the copper species [36]. The findings demonstrate that the AM extract functions not only as a reducing agent but also as an effective stabilizing agent that prevents nanoparticle re-oxidation. Additionally, the absorption at 1087 cm^{-1} serves to corroborate the presence of C-O/O-H groups from polyphenolic compounds that have successfully bound to the copper species. The FTIR spectrum is depicted in Fig. 4.

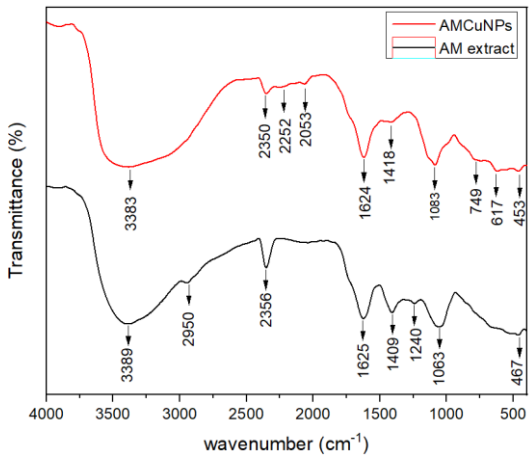

Fig. 4. FTIR of AM extract and AMCuNPs

3.5. X-Ray Diffraction analysis

The results of XRD diffraction analysis on AMCuNPs indicate that the percentage of similarity of Cu(0) formation is less than that of the oxide product. The diffraction of Cu(0) metal has been identified and found with JCPDS (Joint Committee on Powder Diffraction Standards) data No. 96-901-3019 which is found at 2θ values of 42.95˚; 49.91˚; 64.2˚ and 73.27˚. This observation aligns with a previous study that reported metallic copper nanoparticle diffraction peaks at 2θ angles of 43.03˚; 52.05˚ and 73.08˚ [37]. However, the formation percentage of metallic Cu (0) was relatively minor in comparison to the oxidation products, namely CuO, CuO_2 and Cu_2O. In the range of oxidation phases identified, CuO was found to be the most prevalent, exhibiting a distinctive

peak at 2θ angles of 33.53˚; 39.01˚; 48.54˚; 58.19˚; 66.2˚ and 72.29˚. Additionally, a minor, broad reflection was observed at a lower angle around 2θ ≈ 19˚, which was attributed to the amorphous bio-organic matrix or phytochemical residues grom the AM extract that successfully capped the nanoparticles surface. This phenomenon may be attributed to the presence of certain phytochemical compounds in the AM extract that lack capping efficiency, thereby leaving the synthesized AMCuNPs susceptible to rapid re-oxidation. Another contributing factor is the highly reactive nature of copper nanoparticles, which inherently promotes oxidation when exposed to ambient air. The crystallite sizes of both metallic copper and copper oxides were calculated by means of the Debye-Scherrer equation based on the XRD parameters, including the diffraction angles 2θ and Full Width at half Maximum (FWHM) values. Accordingly, the mean crystallite size of the AMCuNPs phases was determinated to be 24.25 nm, 28.41 nm, and 25.58 nm. The XRD spectrum is presented in Fig. 5.

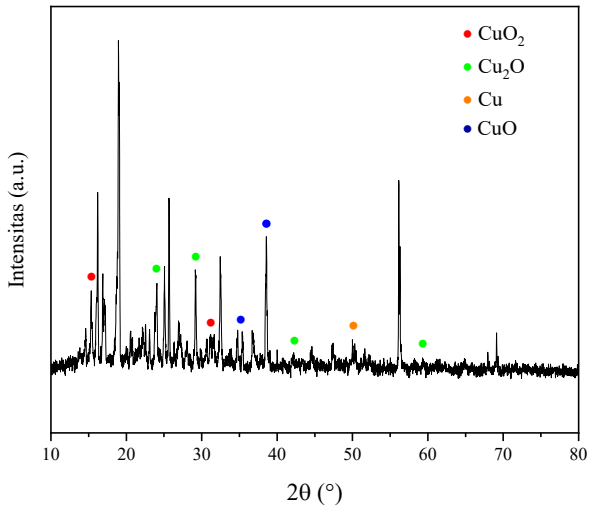

Fig. 5. XRD spectrum of AMCuNP nanoparticles

3.6. SEM–EDS analysis

The surface morphology and elemental composition of the synthesized AMCuNPs were examined using SEM coupled with EDS analysis (Fig. 6(a–c)). SEM micrographs recorded at 5,000× and 10,000× magnifications reveal that the nanoparticles predominantly exhibit a quasi-spherical morphology with heterogeneous particle sizes. The particles appear non-uniformly distributed and there is noticeable agglomeration, likely resulting from high surface energy and insufficient steric stabilization during synthesis. The observed aggregation behavior may be attributed to partial oxidation and limited capping efficiency of phytochemical constituents from the AM extract. In the context of plant-mediated synthesis systems, incomplete surface passivation frequently results in interparticle interactions and cluster formation, particularly under ambient conditions where copper exhibits susceptibility to oxidation.

EDS analysis confirmed the presence of copper as a principal element (16 wt%), along with significant oxygen (62.1 wt%) and carbon (21.8 wt%) signals, as illustrated in Fig. 6(c). The high oxygen content has been demonstrated to significantly support the formation of copper oxide phases (CuO and/or Cu_2O), a finding that is consistent with the XRD results, that demonstrates dominant oxide peaks. The relatively lower proportion of metallic copper suggests partial oxidation of Cu(0) nanoparticles during either the synthesis process or post-synthesis exposure to air. The carbon signal is attributed to residual organic compounds from the *A. muricata* extract, which likely remain adsorbed on the nanoparticle surface and function as stabilizing agents. It is hypothesized that these biomolecular coatings may contribute to nanoparticle formation; however, they might not provide sufficient protection against oxidative transformation.

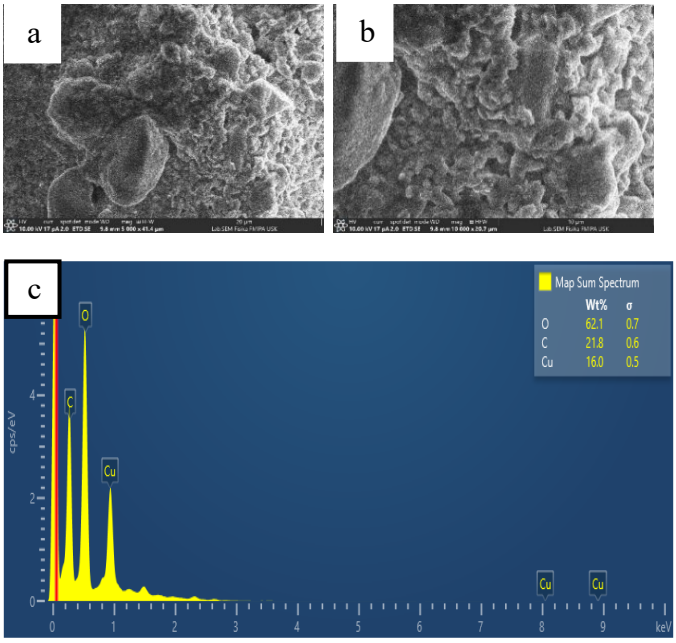

Fig. 6. (a,b) SEM analysis results of AMCuNP nanoparticles at 500x and 10000x scanning images, (c) EDS results of AMCuNP nanoparticles

3.7. TEM analysis

Transmission Electron Microscopy (TEM) was employed to further evaluate the morphology, dispersion, and size distribution of the synthesized AMCuNPs (see Fig. 7(a–c)). The TEM micrographs reveal that the nanoparticles are predominantly spherical and quasi-spherical in morphology, with relatively distinct particle boundaries at the nanoscale. The formation of spherical nanoparticles has been observed in a variety of plant-mediated synthesis systems, as isotropic growth minimizes surface energy and represents a thermodynamically favorable morphology under mild aqueous conditions. Despite their nanoscale dimensions, evidence of partial aggregation is observed, likely due to interparticle interactions and insufficient electrostatic or steric stabilization during synthesis. This observation is consistent with the results of SEM analysis, suggesting that the phytochemical capping agents from the AM extract have only a limited effect on surface passivation. The analysis of particle size as derived from the TEM images (Fig.7(c)) indicates a heterogeneous distribution with a range of approximately 4 to 16 nm. The majority of nanoparticles examined here fall within the 7–10

nm range, indicating that nucleation was dominant during the early stages of the reduction process, followed by limited particle growth. The relatively small particle size is advantageous in terms of enhanced surface area; however, the broad size distribution may influence oxidation behavior and antimicrobial performance.

The nanoscale size observed by TEM appears to be smaller than the crystallite sizes as calculated from XRD analysis. From an instrumental standpoint, the observed discrepancy occurs in view of the significant influence of internal lattice strains on XRD peak broadening. Additionally, the presence of multiple co-existing phases, including Cu (0), CuO, CuO_2 and Cu_2O, contributes to severe peak overlap. It is evident that these factors result in an artificial distortion of the mathematical calculation within the Debye-Scherrer equation, consequently leading to an overestimation of the domain size. Furthermore, while the XRD calculation treats closely aggregated or clustered particles as a single, larger crystalline domain, TEM directly visualizes the true physical boundaries of individual, non-aggregated primary nanoparticles prior to the occurrence of severe agglomeration.

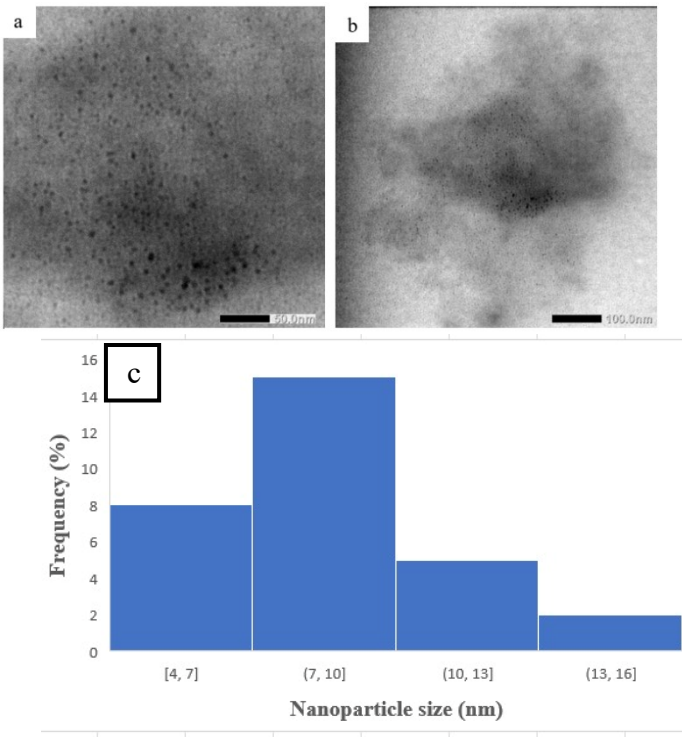

Fig 7. (a,b) TEM of AMCuNPs of 50 nm and 100 nm size (c) Histogram of AMCuNPs particle size distribution

3.8. Antimicrobial activity

The antimicrobial activity of the synthesized AMCuNPs was evaluated against *Staphylococcus aureus* (Gram-positive), *Escherichia coli* (Gram-negative), and *Candida albicans* (fungal strain) using the Kirby–Bauer disc diffusion method (see Fig. 8(a–b)). The inhibition zone diameters are summarized in Table 1. The crude AM extract demonstrated no detectable antimicrobial activity at concentrations of 5%, 10%, or 20%, as no inhibition zones were observed. Similarly, AMCuNPs at concentrations of 5% and 10% exhibited no measurable inhibitory effect against *E. coli* and *S. aureus*. However, at a concentration of 20%, AMCuNPs demonstrated measurable antibacterial activity, producing inhibition zones of 10.16 mm for *S. aureus* and 9.32 mm for E. coli. In contrast, the antifungal activity against *C. albicans* was more pronounced. At a concentration of 10%, an inhibition zone measuring 8.52 mm was observed, while at a concentration of 20%, a substantially larger inhibition zone measuring 27.81 mm was observed, indicating strong antifungal activity at higher dosage.

In accordance with the interpretative criteria outlined by CLSI (2013) – wherein a diameter of ≤14 mm is indicative of resistance -, the inhibition zones observed for *S. aureus* and *E. coli* are classified within the resistant category, thereby signifying a limited antibacterial efficacy. However, the inhibition zone of 27.81 mm against *C. albicans* exceeds the resistant threshold and reflects significant antifungal susceptibility at 20% concentration. The positive controls (chloramphenicol for bacteria and nystatin for fungi) produced inhibition zones ranging from 26.00 to 27.32 mm, thus confirming the reliability of the assay conditions. Nonetheless, it is important to note that while CLSI criteria provide a standard reference point for conventional antibiotics, their application to nanoparticle-based antimicrobial systems should be interpreted with caution due to differing diffusion rates in agar media and multi-targeted mechanisms of action. In comparison to standard pharmaceutical thresholds, the synthesized nanoparticles demonstrated a marked and significantly higher efficacy against fungal strains than bacterial strains.

The relatively low antibacterial performance of AMCuNPs may be attributed to several physicochemical factors identified during the characterization process. SEM and TEM analyses revealed the presence of nanoparticle aggregation, which reduces effective surface area and limits direct interaction with bacterial membranes. Furthermore, XRD and EDS results confirmed the predominance of oxidized copper phases (CuO and Cu_2O) alongside metallic Cu(0). Since metallic Cu(0) typically exhibits higher redox reactivity and enhanced Cu^{2+} ion release, partial oxidation may have diminished antibacterial efficiency. Furthermore, the adsorption of phytochemical residues on the surface of nanoparticle may restrict the release of Cu^{2+} and consequently limit reactive oxygen species (ROS) generation, membrane disruption, and protein denaturation mechanisms.

It is interesting to note that antibacterial activity was slightly higher against the Gram-positive *S. aureus* in comparison to the Gram-negative *E. coli*. This phenomenon may be attributed to the structural differences in cell wall architecture. Gram-negative bacteria possess an outer lipopolysaccharide membrane that acts as a diffusion barrier, thereby reducing nanoparticle penetration and ion uptake.

Conversely, the pronounced antifungal activity against *C. albicans* at a concentration of 20% suggests that copper-based nanoparticles may interact more effectively with fungal cell membranes and intracellular targets. Enhanced susceptibility may be attributed to several factors, including copper-induced oxidative stress, membrane lipid peroxidation, and disruption of fungal enzymatic systems.

Overall, the antimicrobial behavior of AMCuNPs was found to be concentration-dependent, exhibiting limited

antibacterial yet significant antifungal performance activity under the present synthesis conditions. Further optimization of particle dispersion, stabilization, and oxidation control may enhance broad-spectrum antimicrobial efficacy in future investigations.

Table 1. Test Results of AMCuNPs' Antimicrobial Activity against *E. coli*, *S. aureus* and *C. albicans* bacteria

Sample	Zone of Inhibition (mm)		
	S. aureus	*E. coli*	*C. albicans*
AM extract			
5%	-	-	-
10%	-	-	-
20%	-	-	-
AMCuNPs			
5%	-	-	-
10%	-	-	8.52
20%	10.16	9.32	27.81
Control	27.32	27.32	16.00

As depicted in Table 2, the three results of this inhibition zone demonstrate the resistant category in accordance with the Clinical Laboratory Standard Institute (CLSI) (2013).

Table 2, the three results of this inhibition zone demonstrate the resistant category

Inhibition Zone Diameter (mm)	Inhibition Interpretation
≤ 14	*Resistant*
15-18	*Intermediate*
≥19	*Susceptible*

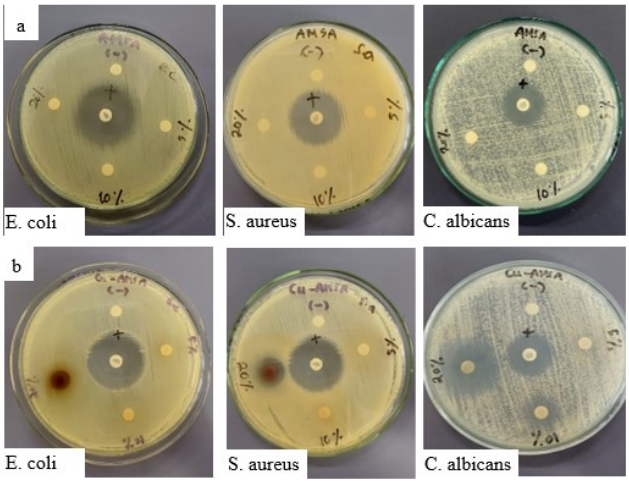

Fig. 8. (a) Antimicrobial activity test results of AM extract (b) Antimicrobial activity test results of AMCuNPs

In comparison to previously reported plant-mediated copper nanoparticle systems, which predominantly produce single-phase CuO with notable antibacterial activity, the present study demonstrates a mixed-phase Cu/Cu_2O/CuO system that exhibits pronounced antifungal selectivity. This suggests that phase composition and oxidation state have a significant effect on the modulation of microbial response, particularly in the enhancement of antifungal performance.

Table 3. Comparison of green-synthesized copper-based nanoparticles utilizing plant extracts and their antimicrobial performance

Study / Plant Source	Metal Type	Particle Size (nm)	Microorganisms Tested	Antimicrobial Activity	Ref.
(Present study)	Cu / Cu_2O / CuO (mixed phase)	4-16	Gram (+): *S. aureus*; Gram (−): *E. coli*; Fungi: *C. albicans*	Weak antibacterial (9–10 mm); strong antifungal (27.81 mm) → selective activity	
Mespilus germanica, *Crataegus spp.*, *Wild barberry* (leaf)	CuO	60–100	Gram (+), Gram (−)	Strong antibacterial; enhanced activity via **synergistic effect**	[38]
Okra (*Abelmoschus esculentus*) fruit	CuO (± Ag doping)	63.3-68.4	Gram (−): *P. aeruginosa*; Fungi: *Candida*, *Rhizopus*, *Aspergillus*	Strong antibacterial (~23 mm); strong antifungal; improved with doping	[39]
Rosmarinus officinalis (leaf)	CuO	18–26	Gram (+): *S. aureus*, *B. cereus*; Gram (−): *E. coli*; Fungi: *C. albicans*	Strong antibacterial (25–26 mm); antifungal (18.1 mm); MIC 1.56–3.12 mg/mL	[40]
Polyalthia longifolia (root)	Cu / Cu_2O / CuO (mixed)	2–10	Gram (+): *S. aureus*; Gram (−): *E. coli*; Fungi: *C. albicans*	Moderate antibacterial (15–17 mm); moderate antifungal (~13.7 mm)	[41]
Annona muricata (bimetallic system)	ZnO–CuO	~ 40	Gram (+), Gram (−)	Strong antibacterial; antioxidant and anticancer	[23]
Annona muricata (leaf extract)	CuO	~ 33.24	Not primary focus	Anticancer activity; antimicrobial not emphasized	[24]

Table 3 presents the comparison in the plant-mediated synthesis of copper-based nanoparticles and their antimicrobial performance among recent studies. The majority of reported systems predominantly produce single-phase CuO nanoparticles with particle sizes ranging from 18 to 100 nm, exhibiting robust and extensive antibacterial activity against both Gram-positive and Gram-negative bacteria. In several cases, enhanced performance is achieved through strategies such as doping (e.g., Ag–CuO) or combining multiple plant-derived nanoparticles, indicating a trend toward improving

activity via compositional or structural modification. Fabrications of engineered nanomaterials, including multi-phase composites and functionalized coatings, have also demonstrated the vital role of tailoring structural configurations in modulating synergistic antibacterial and antimicrobial responses [19,20].

In contrast, studies conducted on mixed-phase copper systems (Cu/Cu_2O/CuO) are relatively limited, with most studies reporting only moderate antimicrobial performance. The present study differs from conventional reports by demonstrating a mixed-phase nanoparticle system with smaller particle size (4–16 nm) and a distinct antimicrobial profile. While the antibacterial activity remains limited, a significantly enhanced antifungal effect against *Candida albicans* is observed. This behavior indicates that phase composition, oxidation state, and surface chemistry play a crucial role in determining microbial selectivity. The comparison demonstrates that, in addition to particle size, the control and tuning of phase composition in green-synthesized copper nanoparticles are pivotal factors determining their antimicrobial functionality, particularly in achieving selective anti-fungal activity.

3.9. Influence of phase composition, oxidation state, and surface properties on antimicrobial activity

The antimicrobial behavior of the synthesized AMCuNPs is found to be highly determined by their phase composition, surface chemistry, and morphology. The presence of mixed phases (Cu, Cu_2O, and CuO) indicates partial oxidation, which affects reactivity and Cu^{2+} ion release. While metallic Cu (0) typically enhances antimicrobial activity, the dominance of oxidized phases likely reduces antibacterial performance but contributes to more stable interactions with microbial cells. Despite the small sizes of nanoparticles (4–16 nm), their antimicrobial efficiency remains constrained, suggesting that particle size is not the sole determining factor. The aaggregation observed in SEM and TEM analyses has been demonstrated to reduce the effective surface area and limit interaction with bacterial cells, particularly for Gram-negative bacteria. Additionally, phytochemical residues from AM extract act as stabilizing agents yet they may also partially block active sites, thereby reducing antibacterial activity. In contrast, a pronounced antifungal effect against *Candida albicans* was observed, suggesting a selective antimicrobial mechanism. This phenomenon may be attributed to differences in fungal cell structure and higher susceptibility to oxidative stress in the presence of copper. In contrast to literature, which typically reports the strong antibacterial activity of single-phase CuO nanoparticles, the present mixed-phase system exhibits distinct antifungal selectivity, highlighting the role of oxidation and phase composition. These findings demonstrate that the observed antimicrobial performance is significantly correlated with the phase composition, aggregation, and surface chemistry, rather than being definitively governed by a single factor. Future work should focus on controlling oxidation state, enhancing dispersion, and investigating Cu^{2+} release and ROS generation to enhance comprehension and optimization of antimicrobial activity.

4. Conclusion

This study successfully demonstrates the green synthesis of copper-based nanoparticles (AMCuNPs) using *A. muricata* stem bark extract as a reducing and stabilizing agent, where the phytochemical content plays a significant role in the reduction process. The synthesized nanoparticles exhibited nanoscale dimensions with quasi-spherical morphology and mixed copper phases (Cu, Cu_2O, and CuO), indicating partial oxidation during synthesis. The antimicrobial evaluation revealed concentration-dependent activity, with relatively low antibacterial effects against *Staphylococcus aureus* (10.16 mm) and *Escherichia coli* (9.32 mm) at a 20% concentration. However, a significantly stronger antifungal response was observed against *Candida albicans* (27.81 mm), suggesting selective interaction with fungal cells. This behavior is likely associated with particle aggregation, surface phytochemical coverage, and phase composition, which may influence ion release and reactivity. The findings highlight the feasibility of plant-mediated synthesis for producing functional copper-based nanomaterials and demonstrate the promising potential of AMCuNPs as selective anti-fungal agents. Further optimization of particle stability and oxidation control is required to improve their broader antimicrobial performance and practical applications.

Authorship contribution statement

Nurjanah; Data curation, formal analysis, investigation, methodology, software, visualization, writing original draft, reviewing and editing, **Irfan Mustafa**; conceptualization, investigation, validation, supervision, writing, reviewing and editing, **Tasya Ulfika**; Writing – review and editing, **Binawati Ginting**; Writing – review and editing and **Ilham Maulana**; writing, reviewing supervision and editing.

Declaration of competing interest

The authors declare that they have no known competing financial interests or personal relationships exist that could have influenced work reported in this article.

Acknowledgments

The authors would like to express their sincere appreciation to Syiah Kuala University that provided academic support, and research facilities that enabled the completion of this study. The authors would like to express their gratitude to Syiah Kuala University for its financial support through the H-Index Research Number: 523/UN11/SPK/PNBP/2019.

Data Availability

The data supporting the findings of this study are accessible within the article.

References

1. A. Pricop, A. Negrea, B. Pascu, N.S. Nemeş, M. Ciopec, P. Negrea, C. Ianăşi, P. Svera, D. Muntean, A. Ivan, I.M. Cristea, *Copper Nanoparticles Synthesized by Chemical Reduction with Medical Applications*. Int. J. Mol. Sci. 26 (2025).

2. B.D. Harishchandra, M. Pappuswamy, G. Shama, V.A. Arumugam, T. Periyaswamy, R. Sundaram, *Copper nanoparticles: a review on synthesis, characterization and applications*. Asian Pacific Journal of Cancer Biology 5 (2020) 201–210.
3. S. Sampaio, J.C. Viana*, Optimisation of the green synthesis of Cu/Cu2O particles for maximum yield production and reduced oxidation for electronic applications*. Materials Science and Engineering: B 263 (2021).
4. J. Leitner, D. Sedmidubský, M. Lojka, O. Jankovský*, The effect of nanosizing on the oxidation of partially oxidized copper nanoparticles*. Materials 13 (2020).
5. Z.X. Chen, Y.J. Song, R.Z. Li, S.J. Guo, L. Shi, Z.R. Yang, X.M. Xue, T. Zhang, *Advances in copper nanocrystals: Synthesis, anti-oxidation strategies, and multiple applications*. Coord. Chem. Rev. 529 (2025).
6. A.I. Osman, Y. Zhang, M. Farghali, A.K. Rashwan, A.S. Eltaweil, E.M. Abd El-Monaem, I.M.A. Mohamed, M.M. Badr, I. Ihara, D.W. Rooney, P.S. Yap, *Synthesis of green nanoparticles for energy, biomedical, environmental, agricultural, and food applications: A review*. Environ. Chem. Lett. 22 (2024) 841–887.
7. H. Singh, M.F. Desimone, S. Pandya, S. Jasani, N. George, M. Adnan, A. Aldarhami, A.S. Bazaid, S.A. Alderhami, *Revisiting the Green Synthesis of Nanoparticles: Uncovering Influences of Plant Extracts as Reducing Agents for Enhanced Synthesis Efficiency and Its Biomedical Applications.* Int. J. Nanomedicine 18 (2023) 4727–4750.
8. M. Bin Mobarak, M.F. Sikder, K.S. Muntaha, S. Islam, S.M.F. Rabbi, F. Chowdhury, *Plant extract-mediated green-synthesized CuO nanoparticles for environmental and microbial remediation: a review covering basic understandings to mechanistic study*. Nanoscale Adv. 7 (2025) 2418–2445.
9. A. Dhaka, S. Chand Mali, S. Sharma, R. Trivedi, *A review on biological synthesis of silver nanoparticles and their potential applications.* Results Chem. 6 (2023).
10. H.R. El-Seedi, M.S. Omara, A.H. Omar, M.M. Elakshar, Y.M. Shoukhba, H. Duman, S. Karav, A.K. Rashwan, A.H. El-Seedi, H.A. Altaleb, H. Gao, A. Saeed, O.A. Jefri, Z. Guo, S.A.M. Khalifa, *Updated Review of Metal Nanoparticles Fabricated by Green Chemistry Using Natural Extracts: Biosynthesis, Mechanisms, and Applications*. Bioengineering 11 (2024).
11. S. Iravani, *Green synthesis of metal nanoparticles using plants*. Green Chemistry 13 (2011) 2638–2650.
12. I.L. Santos, A.M. da C. Rodrigues, E.R. Amante, L.H.M. da Silva, *Soursop (Annona muricata) Properties and Perspectives for Integral Valorization.* Foods 12 (2023).
13. M. Mutakin, R. Fauziati, F.N. Fadhilah, A. Zuhrotun, R. Amalia, Y.E. Hadisaputri, *Pharmacological Activities of Soursop (Annona muricata Lin.).* Molecules 27 (2022).
14. D. Letchumanan, S.P.M. Sok, S. Ibrahim, N.H. Nagoor, N.M. Arshad, *Plant-based biosynthesis of copper/copper oxide nanoparticles: An update on their applications in biomedicine, mechanisms, and toxicity*. Biomolecules 11 (2021).
15. S. Kayalvizhi, A. Sengottaiyan, T. Selvankumar, B. Senthilkumar, C. Sudhakar, K. Selvam, *Eco-friendly cost-effective approach for synthesis of copper oxide nanoparticles for enhanced photocatalytic performance.* Optik (Stuttg). 202 (2020).
16. S. Amaliyah, D.P. Pangesti, M. Masruri, A. Sabarudin, S.B. Sumitro, *Green synthesis and characterization of copper nanoparticles using Piper retrofractum Vahl extract as bioreductor and capping agent*. Heliyon 6 (2020).
17. E. Takele Assefa, G. Shumi, K. Mohammed Gendo, G. Kenasa, N. Roba, *Review on green synthesis, characterization, and antibacterial activity of CuO nanoparticles using biomolecules of plant extract.* Results Chem. 8 (2024).
18. X. Ma, S. Zhou, X. Xu, Q. Du, *Copper-containing nanoparticles: Mechanism of antimicrobial effect and application in dentistry-a narrative review.* Front. Surg. 9 (2022).
19. A.R. Noviyanti, E.N. Asyiah, M.D. Permana, D. Dwiyanti, Suryana, D.R. Eddy, *Preparation of Hydroxyapatite-Titanium Dioxide Composite from Eggshell by Hydrothermal Method: Characterization and Antibacterial Activity.* Crystals (Basel). 12 (2022).
20. L.K. Sakti, G.A.N. Sheha, C.P.S.M. Radhiyah, J. Nugraha, D.R. Eddy, M.D. Permana, I.P. Maksum, Y. Deawati, *Cotton Fabric Coating by rGO and Polymethylsiloxane Layer with Antibacterial, Hydrophobic and Photothermal Properties.* Trends in Sciences 20 (2023).
21. J.Y. Park, S. Lee, Y. Kim, Y.B. Ryu, *Antimicrobial Activity of Morphology-Controlled Cu2O Nanoparticles: Oxidation Stability under Humid and Thermal Conditions.* Materials 17 (2024).
22. L. Wang, C. Hu, L. Shao, *The antimicrobial activity of nanoparticles: Present situation and prospects for the future.* Int. J. Nanomedicine 12 (2017) 1227–1249.
23. K. Madeshwaran, R. Venkatachalam, *Green synthesis of bimetallic ZnO–CuO nanoparticles using Annona muricata l. extract: Investigation of antimicrobial, antioxidant, and anticancer properties.* Journal of Industrial and Engineering Chemistry 140 (2024) 454–467.
24. R.I. Mahmood, A.A. Kadhim, S. Ibraheem, S. Albukhaty, H.S. Mohammed-Salih, R.H. Abbas, M.S. Jabir, M.K.A. Mohammed, U.M. Nayef, F.A. AlMalki, G.M. Sulaiman, H. Al-Karagoly, *Biosynthesis of copper oxide nanoparticles mediated Annona muricata as cytotoxic and apoptosis inducer factor in breast cancer cell lines.* Sci. Rep. 12 (2022).
25. I. Maulana, B. Ginting, K. Azizah, *Green synthesis of copper nanoparticles employing Annona squamosa L extract as antimicrobial and anticancer agents.* S. Afr. J. Chem. Eng. 46 (2023) 65–71.
26. I. Maulana, D. Fasya, B. Ginting, *Biosynthesis of Cu nanoparticles using Polyalthia longifolia roots extracts for antibacterial, antioxidant and cytotoxicity applications.* Materials Technology 37 (2022) 2517–2521.
27. G.I. Edo, A.N. Mafe, A.B.M. Ali, P.O. Akpoghelie, E. Yousif, E.F. Isoje, U.A. Igbuku, K. Zainulabdeen, J.O. Owheruo, A.E.A. Essaghah, H. Umar, D.S. Ahmed, A.A. Alamiery, *Eco-friendly nanoparticle phytosynthesis via plant extracts: Mechanistic insights, recent advances, and multifaceted uses.* Nano TransMed 4 (2025).
28. A.N. Labaran, Z.U. Zango, G. Tailor, A. Alsadig, F. Usman, M.T. Mukhtar, A.M. Garba, R. Alhathlool, K.H. Ibnaouf, O.A. Aldaghri, *Biosynthesis of copper nanoparticles using Alstonia scholaris leaves and its antimicrobial studies.* Sci. Rep. 14 (2024).
29. R. Amjad, B. Mubeen, S.S. Ali, S.S. Imam, S. Alshehri, M.M. Ghoneim, S.I. Alzarea, R. Rasool, I. Ullah, M.S. Nadeem, I. Kazmi, *Green synthesis and characterization of copper nanoparticles using fortunella margarita leaves.* Polymers (Basel). 13 (2021).
30. H.T. Gebrie, M.A. Assege, D.S. Meshesha, B.A. Tebeje, G.W. Moges, A.T. Wodajo, G.M. Manahelohe, A.A. Belew, *Biosynthesis and characterization of copper oxide nanoparticles from Plumbago zeylanica leaf extract for antibacterial and antioxidant activities.* Sci. Rep. 15 (2025).
31. M. V. Faustino, M.A.F. Faustino, H. Silva, Â. Cunha, A.M.S. Silva, D.C.G.A. Pinto, *Puccinellia maritima, Spartina maritime, and Spartina patens Halophytic Grasses: Characterization of polyphenolic and chlorophyll profiles and evaluation of their biological activities*. Molecules 24 (2019).
32. Y. Yu, L. Zhang, J. Wang, Z. Yang, M. Long, N. Hu, Y. Zhang, *Preparation of hollow porous Cu_2O microspheres and photocatalytic activity under visible light irradiation*. Nanoscale Res. Lett. 7 (2012).
33. N. Munandar, H.F. Aritonang, R. Bonaventura, D.P. Wijaya, *Synthesis of Cu Nanoparticles using Anredera cordifolia Extract and their Potential as Antidiabetic with Alpha Amylase Enzyme Inhibition*. Communications in Science and Technology 10 (2025) 422–430.
34. S. Nareshkumar, K. Madhivanan, A.K. Sundramoorthy, *Development of a hybrid nanomaterial-based electrochemical sensor for the determination of L-tyrosine using copper oxide and SWCNTs.* Journal of SolidState Electrochemistry (2026).
35. E.A. Mohamed, *Green synthesis of copper & copper oxide nanoparticles using the extract of seedless dates*. Heliyon 6 (2020).
36. H.M. Albert, C.A. Gonsago, *Green Procedure for the synthesis of Copper Nanoparticles using Nerium oleander Leaf Extract: Characterizations and Applications.* Oriental Journal Of Chemistry 39 (2023) 792–797.
37. akl awwad and mohammad amer, *Green Synthesis of Copper Nanoparticles by Citrus Limon Fruits Extract, Characterization and Antibacterial Activity.* International Scientific Organization 7 (1) (2021)

1-8.

38. H. Koohestani, A. Balooch, H. Staji, *Biosynthesis of CuO-nanoparticles using extracts of Mespilus germanica, Crataegus spp., and Wild barberry and their synergistic antibacterial activity.* Giant 26 (2025).
39. M.J. Javid-Naderi, Z. Sabouri, A. Jalili, H. Zarrinfar, S. Sammak, M. Darroudi, *Green synthesis and characterization of Ag/CuO nanoparticles: Exploring their antifungal, antimicrobial, and cytotoxic properties.* Environ. Technol. Innov. 38 (2025).
40. M.D. Moroda, T. Leta Deressa, A.H. Tiwikrama, T.F. Chala, *Green synthesis of copper oxide nanoparticles using Rosmarinus officinalis leaf extract and evaluation of its antimicrobial activity.* Next Materials 7 (2025).
41. I. Maulana, B. Ginting, I. Mustafa, R.A.N. Islami, *Green Synthesis of Copper Nanoparticles Using Polyalthia longifolia Roots and their Bioactivities Against Escherichia coli, Staphylococcus aureus, and Candida albicans.* J. Pharm. Bioallied Sci. 16 (2024) S2218–S2223.